CHAPTER IV: Experimental and Numerical Results

4.1. Case 1: Dambreak Flow through without obstacle

Figure 12 shows the schematic diagram of the computational domain (length 1.90 m, width 0.16 m and height 0.40 m). For computational Grid 1: the mesh was 268 × 40 × 80 in x, y and z diection, respectively.

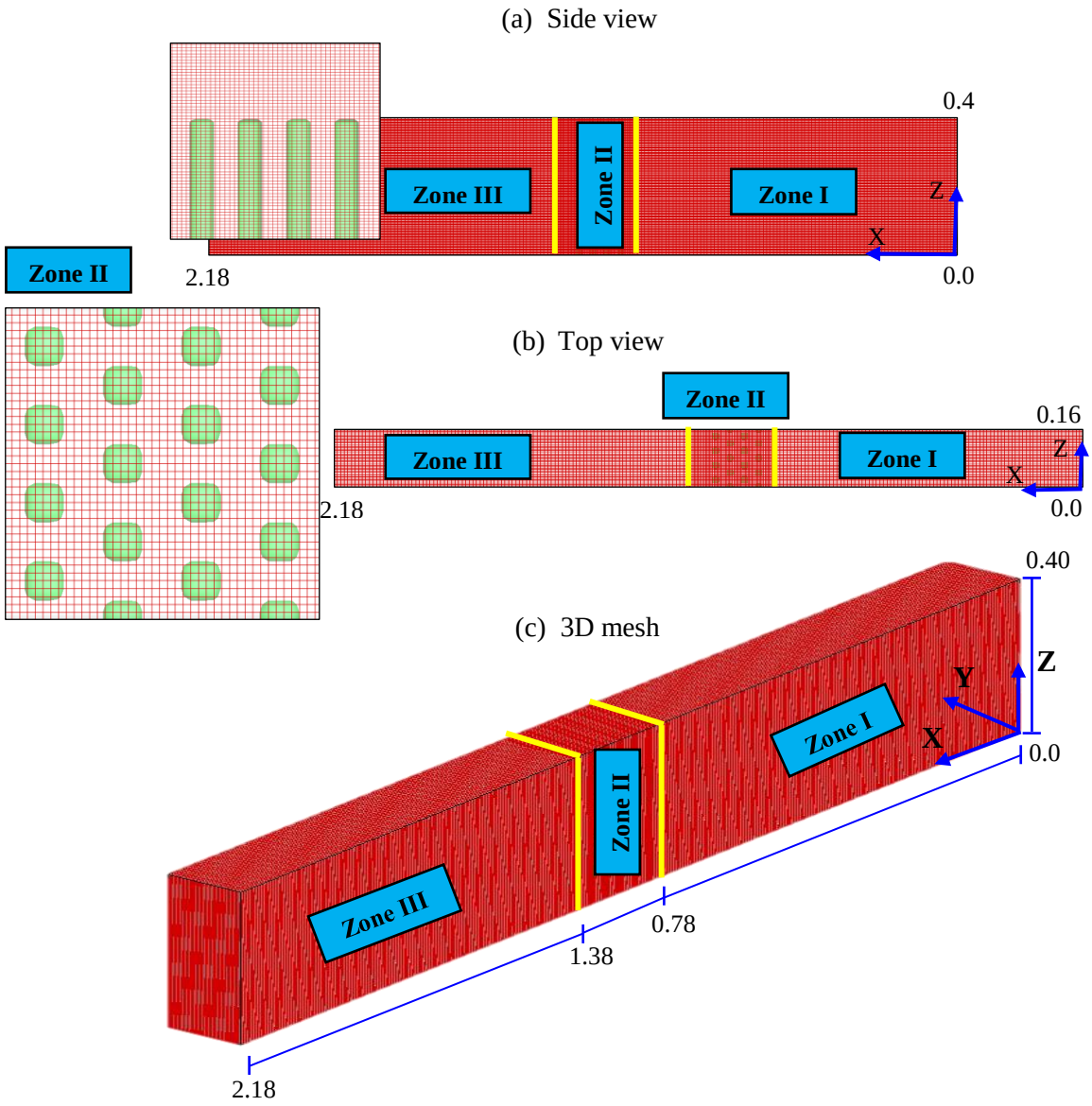

Figure 12. Computational domain and grid arrangement of grid A and the obstacle installed in zone II. (smallest grid size: Δx = 4 mm; Δy = 4 mm; Δz = 5 mm in zone II).

The stretching ratios equal to 1.0 for all three zones (uniform, orthogonal grid in all three zones). The smallest grid size was in zone II: $\Delta x = 4$ mm, $\Delta y = 4$ mm and $\Delta z = 5$ mm. The average time step was $\Delta t = 5 \times 10^{-4}$ sec. The grid sensitivity was checked by comparing the simulation results and computational times of three different grids for Case 1 (Table 1).

Table 1. Flow parameters of the flume experiments.

Case	h_o (m)	h_1(m)	C_s	Porous models	h_f (m)
1	0.26	0.02	0.15	-	-
2	0.26	0.02	0.15	Solid obstacle	0.05
3	0.26	0.02	0.15	1. Solid obstacle 2. Carman-Koseny 3. Forchheimer	0.10
4	0.26	0.02	0.15	Forchheimer	0.20

The length, width and height of the flume are 2.18, 0.16 m and 0.40 m. The staggered obstacle with 0.16 m by 0.16 m at located centrally at x = 0.78 m.

The no-slip boundary condition is applied at the bottom of the flume. The free-slip boundary conditions is applied at side walls of the flume. On the free surface, the zero pressure boundary condition is employed. In addition, no flux boundary condition is set at the outlet of the computational domain. The initial water depth behind the sliding gate was $h_o = 0.26$ m, and the initial water depth in the flume was $h_1 = 0.02$ m.

The difference Δ is defined as:

$$\Delta = \left| \frac{\eta_p - \eta_m}{\eta_p} \right| \times 100\% \qquad (11)$$

where η_m is the measured wave height, η_p is the predicted wave height.

The maximum η_{max} and time-averaged wave heights $\bar{\eta}$ (measured at a distance and 40 mm to the sidewalls) were computed from the simulation results between 0 ~ 1.4 sec.

The time-averaged wave height is calculated as:

$$\bar{\eta}=\frac{1}{n}\sum_{i=1}^{n}\eta_{p,i} \tag{12}$$

where $\eta_{p,i}$ is the predicted wave height at time t = 0.1 x i sec at location x = 1.18 m and the total data number n = 14.

Table 2. Simulation results of different computational grids for Case 1.

		Grid A	**Grid B**	**Grid C**
smallest grid size (mm)		Δx = 4 Δy = 4 Δz = 5	Δx = 3 Δy = 4 Δz = 4	Δx = 4 Δy = 4 Δz = 2
Total grid number		857,600 268×40×80	1,144,800 318×40×90	1,500,800 268×40×140
Wave height	Measured $\bar{\eta}$, η_{max} (m)	0.0411, 0.0751		
	Predicted $\bar{\eta}$, η_{max} (m)	0.0439, 0.0800	0.0439, 0.0826	0.0434, 0.0810
	Δ	**4.9%, 6.2%**	**6.5%, 9.1%**	**5.2%, 7.4%**
$\overline{\Delta t}$ (sec)		0.0005	0.0006	0.0004
Computational time		10.4 hr	16.0 hr	43.2 hr

As can be seen in Table 2, the difference between the simulated and measured maximum wave heights η of Grid A, Grid B, Grid C, were Δ = 6.2%, 9.1%, 7.4%, respectively. Therefore, Grid C (268×40×140) was used for the simulation, and the wave heights were shown in Figure 13.

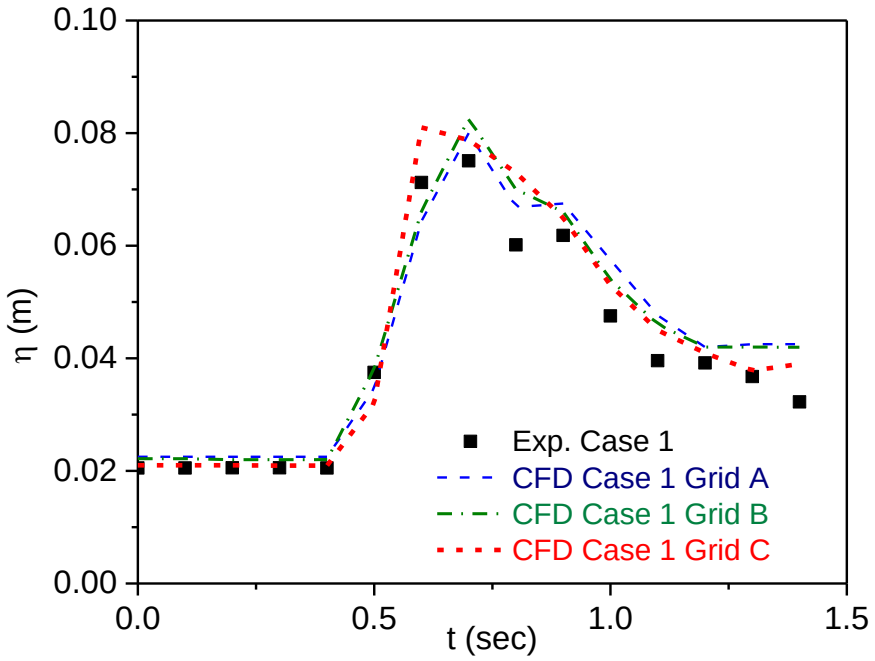

Figure 13. Comparison of measured and simulated wave heights of different computational grids for Case 1 (without obstacle).

Figure 14 and Table 3 compare the simulated wave heights of different Courant numbers. The Courant number is defined as:

$$\mathrm{Cr} = \frac{V \cdot \Delta t}{\Delta x} \tag{13}$$

where Δt is the time step, Δx is the spacing of the grid in the numerical model, and V is the fluid velocity.

The differences Δ between the measured and simulated average wave heights η of Cr = 0.5, Cr = 0.7, Cr = 0.9 were Δ = 8.8%, 7.1%, 6.1%, respectively. The differences between the measured and simulated maximum wave heights were Δ = 9.6%, 6.2% and 6.2% for Cr = 0.5, Cr = 0.7, Cr = 0.9, respectively. The Courant number Cr = 0.9 was used for all cases of the simulation to obtain a sufficient precision and to save the computational time.

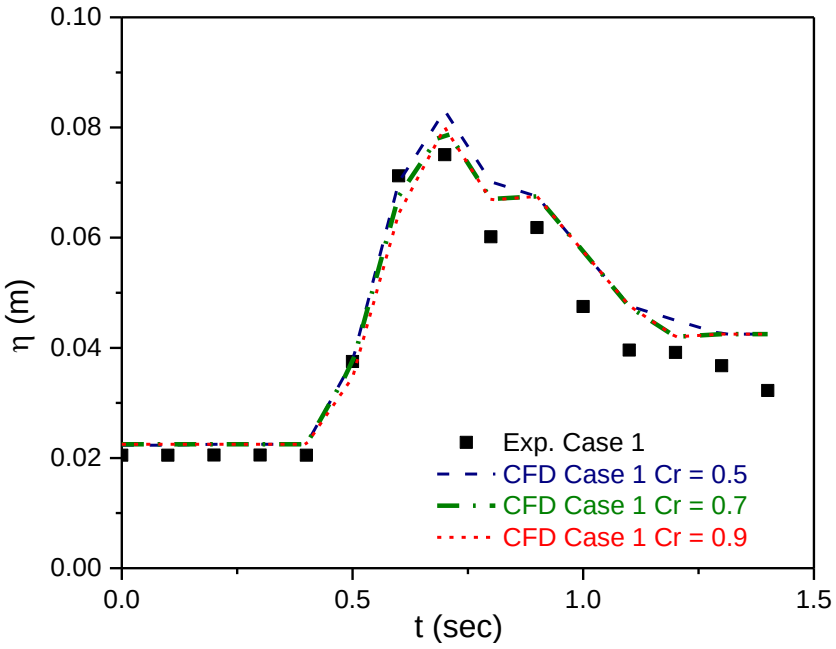

Figure 14. Simulation results of different Courant numbers for Case 1 without obstacle. The initial water depth behind the gate h_o = 0.26 m; in flume h_1 = 0.02 m.

Table 3. Simulation results of different Courant numbers for Case 1.

Case		**1**	**1**	**1**
Cr		0.5	0.7	0.9
Total grid number		857,600 268×40×80	857,600 268×40×80	857,600 268×40×80
Wave height	Measured $\bar{\eta}$, η_{max} (m)		0.0411, 0.0751	
	Predicted $\bar{\eta}$, η_{max} (m)	0.0450, 0.0831	0.0443, 0.0800	0.0439, 0.0800
	Δ	**8.8%, 9.6%**	**7.1%, 6.2%**	**6.3%, 6.2%**
$\overline{\Delta t}$ (sec)		0.0004	0.0005	0.0005
Computational time		17.0 hr	12.3 hr	10.4 hr

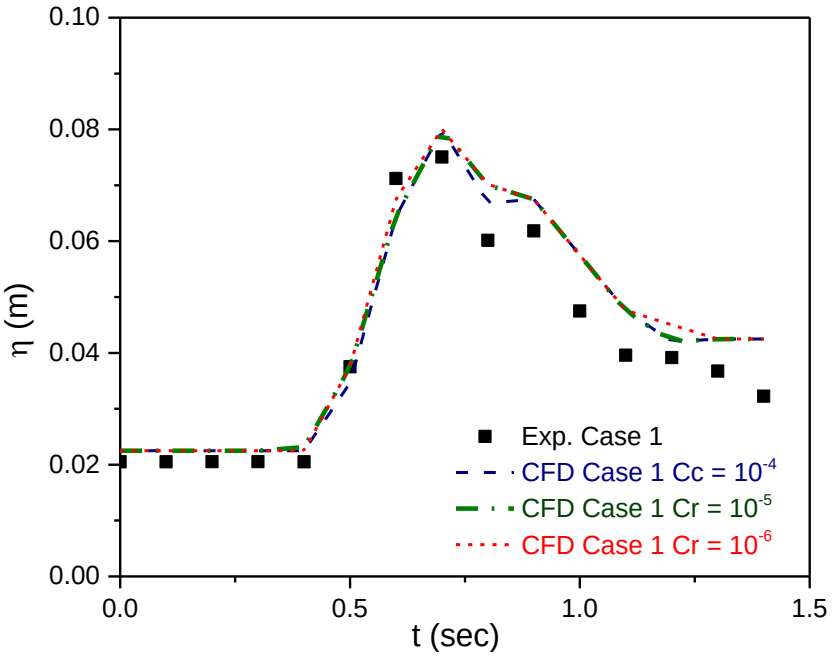

Figure 15. Simulation results of different convergence criterion for Case 1.

Table 4. Simulation results of different convergence criterion for Case 1.

		Case 1 Grid A	**Case 1 Grid A**	**Case 1 Grid A**
Convergence Criterion		1.0e-4	1.0e-5	1.0e-7
Total grid number		857,600 268×40×80	857,600 268×40×80	857,600 268×40×80
Cr		0.9	0.9	0.9
Wave height	Measured $\bar{\eta}$, η_{max} (m)		0.0411, 0.0751	
	Predicted $\bar{\eta}$, η_{max} (m)	0.0439, 0.0800	0.0443, 0.0800	0.0447, 0.0800
	Δ	**6.3%, 6.2%**	**7.2%, 6.2%**	**8.0%, 6.2%**
$\overline{\Delta t}$ (sec)		0.0005	0.0005	0.0007
Computational time		10.4 hr	11.3 hr	9.4 hr

Figure 15 compares the simulated wave heights using different convergence criterion. The differences (see Table 4) between the measured and simulated average wave heights η for Cc = 1.0 x 10^{-4}, 1.0 x 10^{-5}, 1.0 x 10^{-6} were Δ = 6.3%, 7.2%, 8.0%, respectively. Therefore, the convergence criterion Cc = 1.0 x 10^{-4} was used for all cases of the simulation. The Smagorinsky constant Cr = 0.15 was used for all cases of the simulation.

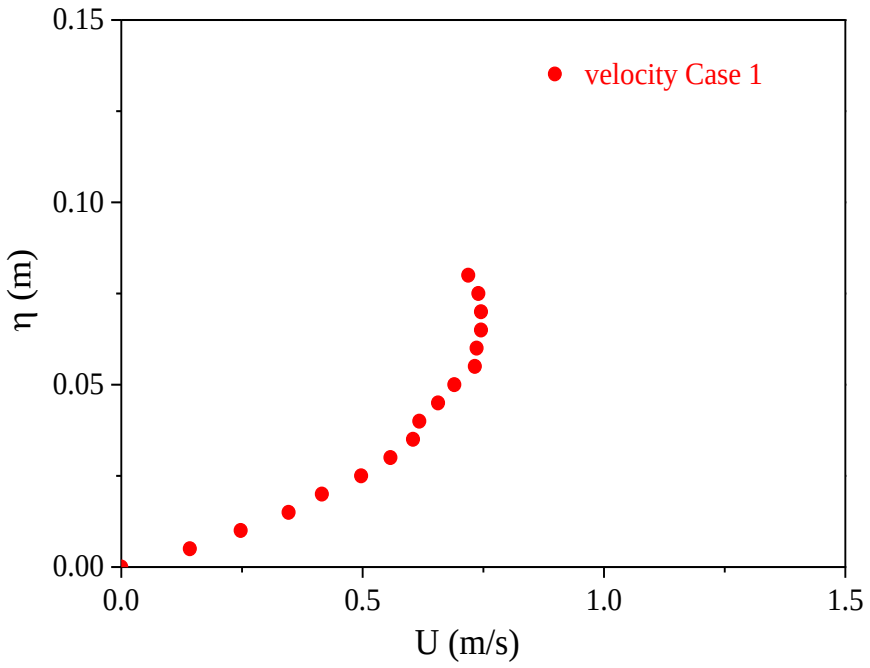

Figure 16. Profiles of instantaneous velocity on the central plane at location x = 1.18 m, y = 0.08 m when t = 0.70 sec for Case 1 (without obstacle).

Figure 16 shows the simulated instantaneous velocity at time t = 0.7 sec and location x = 1.18 m, y = 0.08 m for Case 1. The velocity at the channel bed U = 0.0 m/s, this is because the boundary conditions of the channel bed is a no-slip boundary. The maximum velocity between depth z = 0.0 ~ 0.080 m was about 0.75 m/s. Because Case 1 is dambreak flow without obstacle, the characteristic velocity of the dambreak flow is $U_o = \sqrt{gh_o}$. When the initial water depth h_o = 0.26 m, and the characteristic velocity U_o = 1.60 m/s. The simulated velocity is smaller than the characteristic velocity due to the bed friction. Figure 17 illustrated velocity vectors on the central plane (y = 0.08 m) of the flume at six different

times from t = 0.5~1.0 sec.

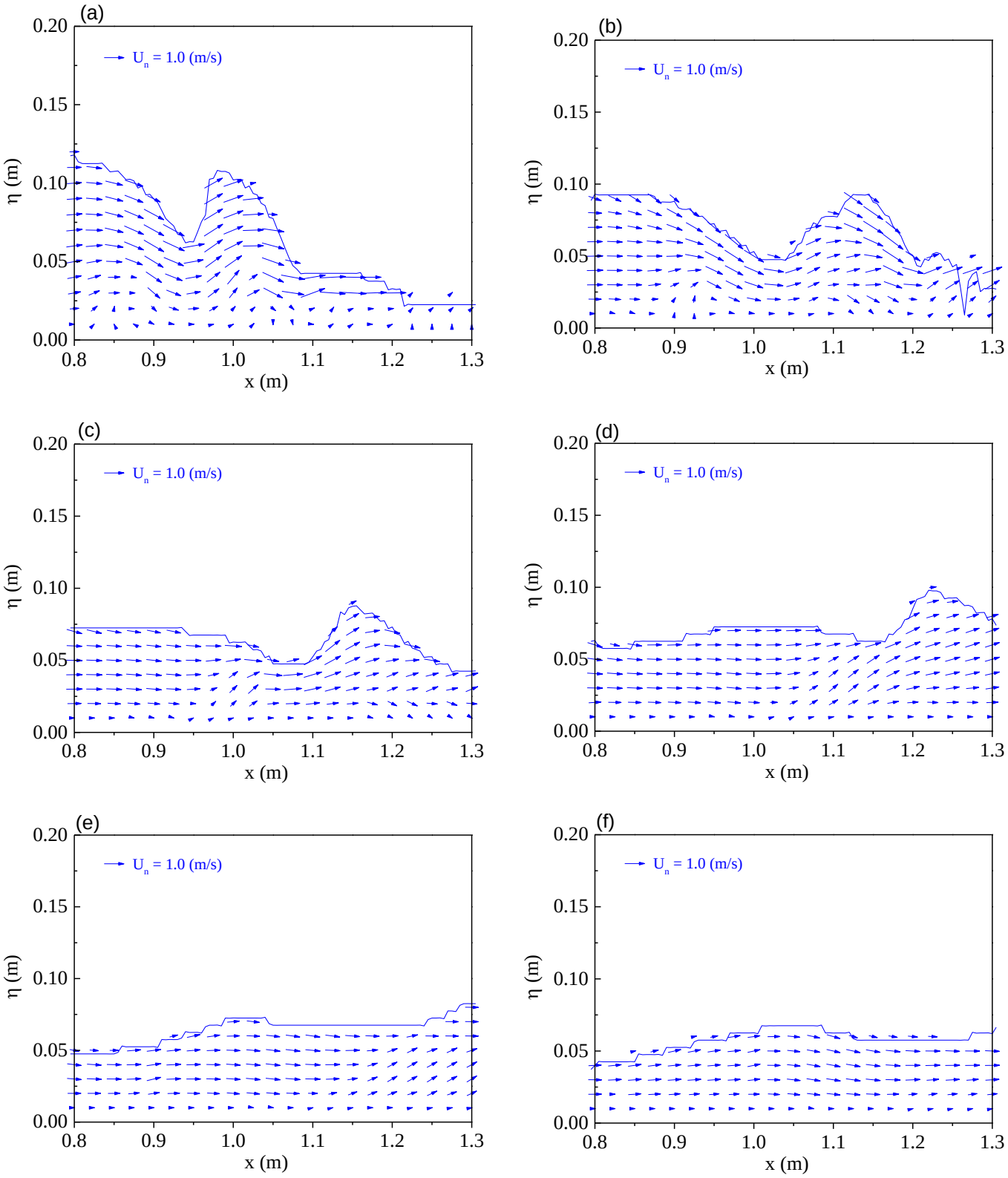

Figure 17. Velocity vectors on the central plane (y = 0.08 m) of the flume for Case 1 (without obstacle). (a) t = 0.5 s; (b) t = 0.6 s; (c) t = 0.7 s; (d) t = 0.8 s; (e) t = 0.9 s; and (f) t = 1.0 s.

4.2. Case 2: Dambreak Flow through a solid obstacle

The initial water depth behind the gate was h_0 = 0.26 m, in the flume was h_1 = 0.02 m. The length of the obstacle was 0.16 m, and obstacle height was 0.05 m. The computational mesh was 268 × 40 × 80. The smallest grid size was in Zone II: Δx = 4 mm, Δy = 4 mm and Δz = 5 mm. The stretching ratio in Zone I was 1.0, Zone II was 1.0, Zone III was 1.0. The grid sensitivity was checked by comparing the simulation results of three different grids the same flow condition. The average time step was $\Delta t = 5 \times 10^{-4}$ sec.

The flow parameters of the validation cases are listed in Table 5. The wave height η were calculated from the simulation results between 0 ~ 1.4 sec. As can be seen in Table 6, the relative differences between the simulated and measured average wave heights η of Grid A, Grid B, Grid C were Δ = 7.1%, 12.8%, and 4.7%, respectively. In Case 2, grid C showed good result with the least error value (see Figure 18).

Table 5. Information of parameters used for simulation.

Parameters	Values
output dt (sec)	0.1 sec
Courant number	0.90
Convergence criterion	1.0×10^{-4}
dt_init, dt_grow, dt_min, dt_max	1.0×10^{-6}, 1.1, 1.0×10^{-7}, 1.0
water density (kg/m^3)	1000
inviscid, turbulence_model	false, LES
Smagorinsky coefficient (Cs)	0.15
porous_flow, permeability constant C, α, β	true, 3000, 500, 1.1

Table 6. Simulation results of different computational grids for Case 2.

		Grid C
smallest grid size (mm)		Δx = 4 Δy = 4 Δz = 2
Total grid number		1,500,800 268×40×140
Wave height	Measured $\bar{\eta}$, η_{max} (m)	0.0481, 0.1314
	Predicted $\bar{\eta}$, η_{max} (m)	0.0501, 0.1378
	Δ	**4.0%, 4.7%**
$\overline{\Delta t}$ (sec)		0.0002
Computational time		53.6 hr

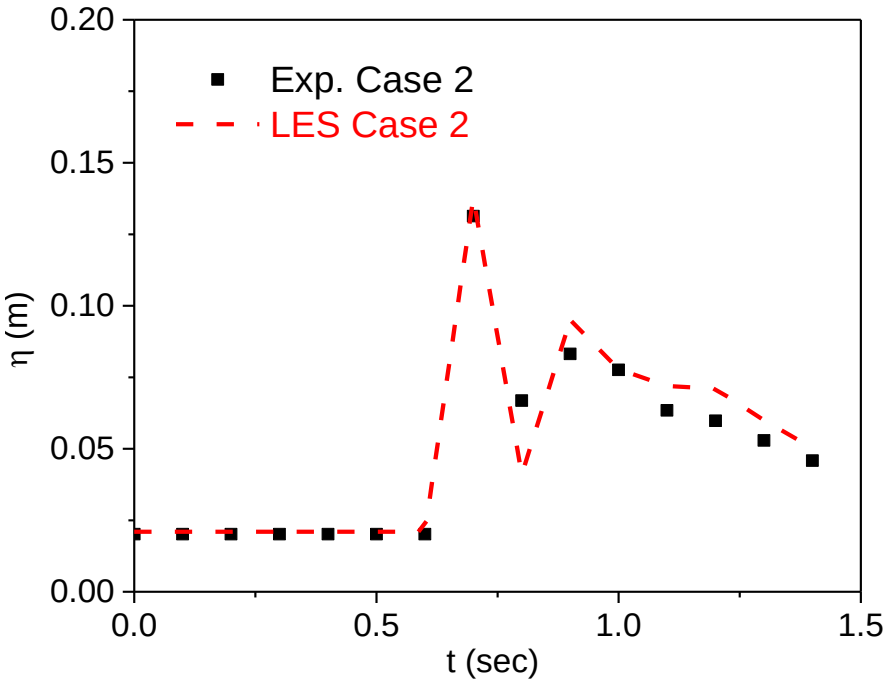

Figure 18. Comparison of measured and simulated wave heights of Case 2.

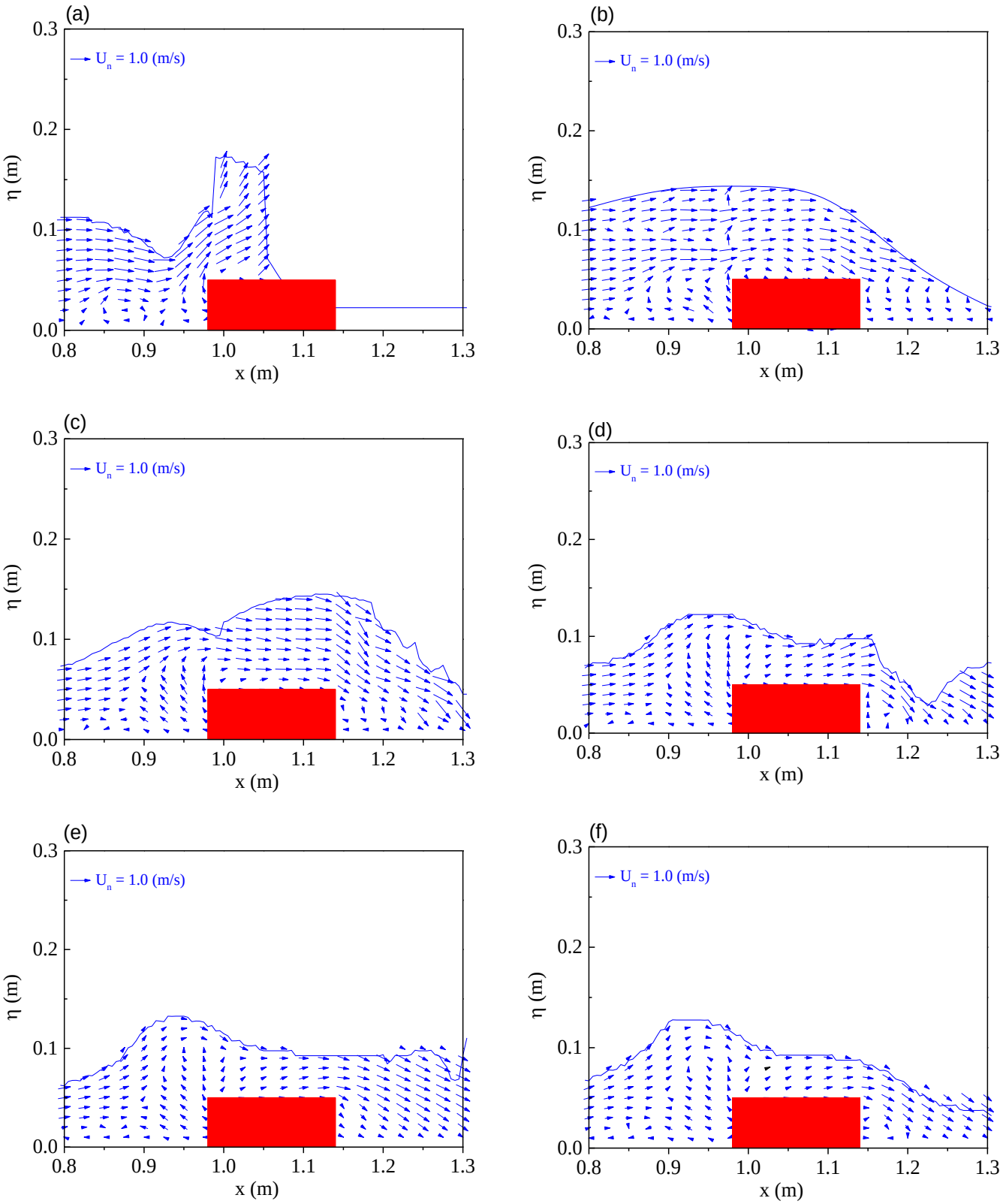

Figure 19. Velocity vectors on the central plane (y = 0.08 m) for Case 2 (solid obstacle, h_f = 0.05 m). (a) t = 0.5 s; (b) t = 0.6 s; (c) t = 0.7 s; (d) t = 0.8 s; (e) t = 0.9 s; (f) t = 1.0 s.

Figure 19 illustrates the simulated velocity vectors on the central plane (y = 0.08 m) of the flume at six different times from t = 0.5 ~ 1.0 sec. Figure 20 shows profiles of instantaneous horizontal velocity after obstacle on the central plane of the flume (x = 1.18 m, y = 0.08 m) at time t = 0.7 sec. Case 2 is the dambreak flow with a solid obstacle, when the wave hit the obstacle, then a hydraulic jump appeared at the downstream side. This phenomenon caused the velocity on the downstream increased rapidly.

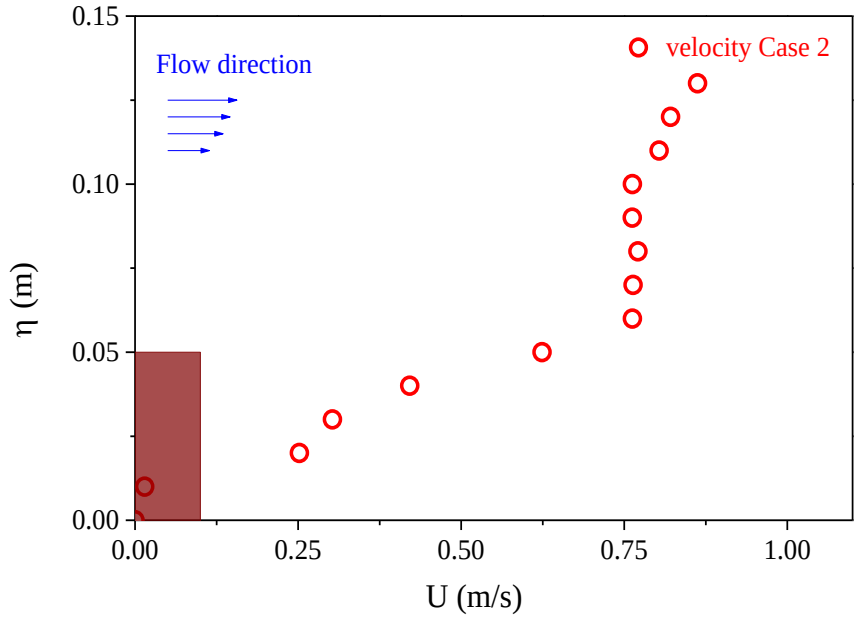

Figure 20. Profiles of instantaneous velocity after obstacle on the central plane of the flume (x = 1.18 m, y = 0.08 m) for Case 2 (solid obstacle).

Figure 21 shows the profile of horizontal velocity upstream of the obstacle on the central plane of the flume (x = 1.18 m, y = 0.08 m) at time t = 0.7 sec. The upstream velocity changed before obstacle does not occur, only a little effect on the flow behind the wave before the wave front hit the obstacle.

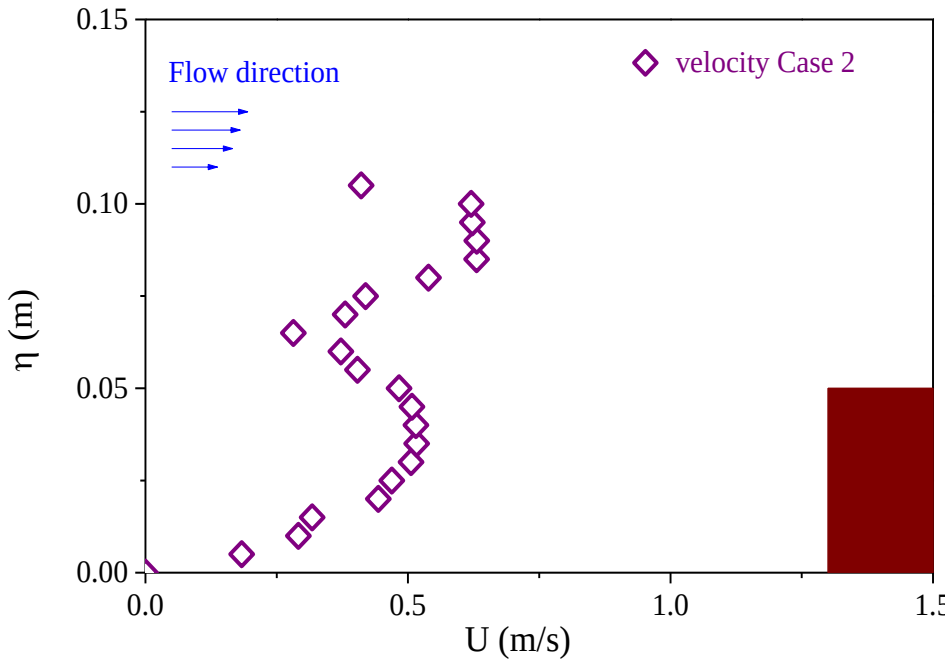

Figure 21. Profiles of instantaneous velocity before obstacle on the central plane of the flume (x = 0.92 m, y = 0.08 m) for Case 2 (solid obstacle).

4.3. Case 3 and Case 4: Dambreak flow through porous obstacles

This section investigates a three-dimensional dambreak flow interacting with porous obstacles. However, few experiments have been conducted for these situations. Similar to the Case 1 and 2, there was no difference in the boundary condition. The Smagorinsky coefficient was set as Cs = 0.15. The initial water depth was h_0 = 0.26 m, obstacle height was 0.10 m (Case 3) and 0.20 m (Case 4). The computational mesh was 268 × 40 × 80. The smallest grid size was in Zone II: Δx = 4 mm, Δy = 4 mm and Δz = 5 mm.

The porosity is defined as:

$$n = \frac{Area\ of\ solid}{Cross\text{-}sectional\ area\ of\ channel\ flow} \tag{14}$$

For Case 3 and 4, the porosity of the obstacles is 0.5.

The wave height η were calculated from the simulation results between 0 ~ 1.4 sec. Figure 22 compares the measured and simulated wave heights of Case 3 that uses solid

method. In this simulation, the obstacles were solid, square cylinders and were installed one by one in accordance with their actual positions.

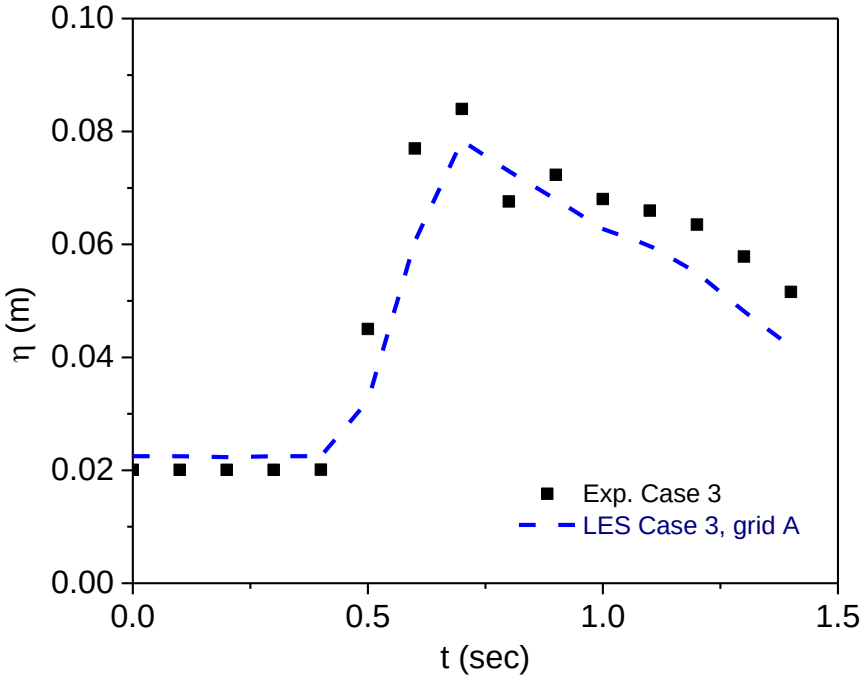

Figure 22. Comparison of measured and simulated wave heights uses solid method for Case 3 at x = 1.18 m and y = 0.08 m, h_f = 0.10 m. The square cylinders are installed in their actual positions.

This method uses grid A and grid B. The relative differences between the simulated and measured of maximum wave heights η_{max} of Grid A and Grid B were Δ = 28.4%, and 21.0%, respectively. The differences between the simulated and measured average wave heights η of Grid A and Grid B were Δ = 36.3%, and 33.4%, respectively. The results indicate a major fault, the fault is probably caused by insufficient resolution of the computational grid. Therefore, the effect of obstacles on the dambreak flow was simulated by a porous drag model.

The drag force, f_d, in the direction of the flow can be calculated by the Darcy law (Carman-Kozeny, 1937):

$$\vec{f}_d = -C \cdot \frac{(1-n)^2}{n^3} \vec{u}_n \qquad (15)$$

where n is the porosity of the obstacle; u_n is the directional velocity; and C is the permeability constant.

Figure 23 and Table 7 compare the measured and simulated wave heights of Case 3 by the drag model of Carman-Kozeny (1937) with the permeability constant C = 1800 and 3000. The porous obstacle can be simulated by coarse grid, so the grid A was used for the simulation. The differences between the simulated and measured average wave heights η was Δ = 4.5% for C = 1800, Δ = 1.1% for C = 3000. The differences between the simulated and measured maximum wave heights η was Δ = 13.7% for C = 1800, Δ = 10.1% for C = 3000.

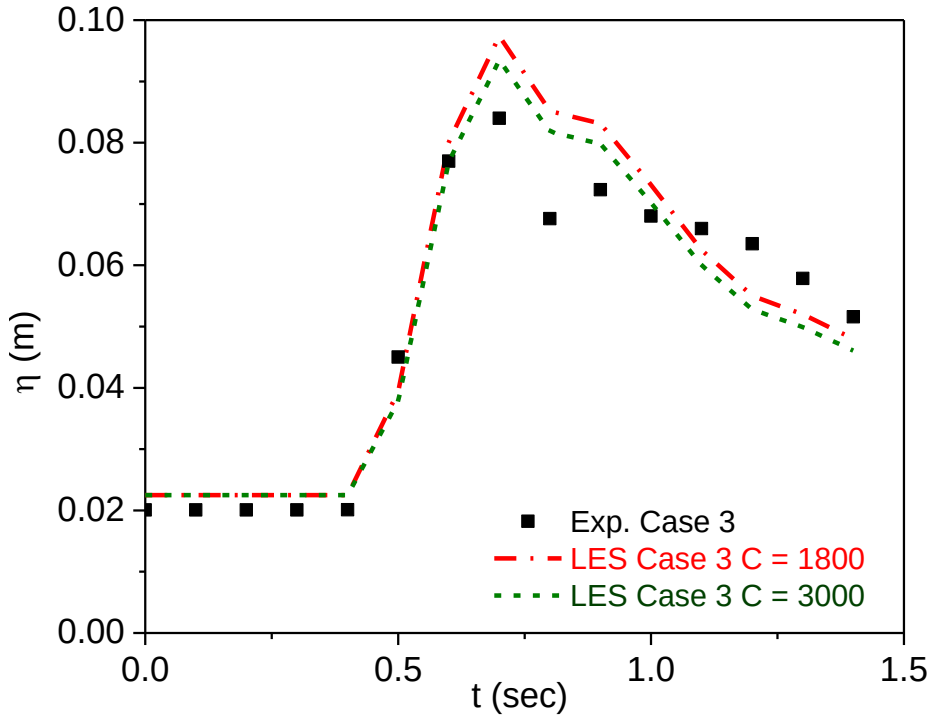

Figure 23. Comparison of measured and simulated wave heights for Case 3 (short porous obstacles) at location x = 1.18 m and y = 0.08 m using the drag function of Carman-Kozeny (1937).

Table 7. Simulation results of short porous obstacle Case 3 with Caman-Kozeny method.

		Grid A	**Grid A**
smallest grid size (mm)		Δx = 4 Δy = 4 Δz = 5	Δx = 4 Δy = 4 Δz = 5
Total grid number		857,600 268×40×80	857,600 268×40×80
Permebaility constant C		1800	3000
Wave height	Measured $\bar{\eta}$, η_{max} (m)	0.0502, 0.0840	
	Predicted $\bar{\eta}$, η_{max} (m)	0.0526, 0.0974	0.0508, 0.0935
	Δ	**4.5%,** **13.7%**	**1.1%,** **10.1%**
$\overline{\Delta t}$ (sec)		0.0004	0.0004
Computational time		21.9 hr	22.8 hr

Forchheimer (1901) added an inertia term to Darcy's equation for high Reynolds number flows in porous media:

$$\vec{f}_d = -\alpha \cdot \frac{(1-n)^2}{n^3} \vec{u}_n - \beta \cdot \frac{(1-n)}{n^3} \vec{u}_n^2 \tag{16}$$

where α is the permeability constant where β is the inertia factor (dimensionless), and the other formula can be seen in Table 8.

Figure 24 compares the measured and simulated wave heights using the drag model of Forchheimer (1901) for Case 3 at location x = 1.18 m and y = 0.08 m. There are several

references for the values of α and β. This study set the permeability constant α = 500 and the inertia factor β = 1.1 by comparing with the measured water surfaces of Case 3. The difference between the simulated and measured average wave heights η was Δ = 5.6% at location x = 1.18 m (see Table 9 for detail). The difference between the simulated and measured maximum wave heights η was Δ = 4.0% at time t = 0.6 sec.

Table 8. Some reference to determine the value of porous drag (f_d)

Perry, Gree, and Maloney (1984)	$\vec{f}_d = \frac{1}{C^2}\frac{\left(A_p / A_f\right)^2 - 1}{t}$
Miguel et al. (1997)	$\vec{f}_d = \frac{1}{\rho}\frac{\partial P}{\partial x} = \frac{\nu}{K}\vec{u}_n + \left(\frac{Y}{\sqrt{K}}\right)\vec{u}_n^2$
Liu et al., 1999 van Gent, 1995 Lara et al., 2011 Wu and Hsiao, 2013	$f_d = -\alpha\nu\cdot\frac{(1-n)^2}{n^3 D_{50}^2}u_n - \beta\cdot\frac{(1-n)}{n^3 D_{50}^2}u_n^2$
Pramukti (2017)	$\vec{f}_d = -\alpha\cdot\frac{(1-n)^2}{n^3}\vec{u}_n - \beta\cdot\frac{(1-n)}{n^3}\vec{u}_n^2$

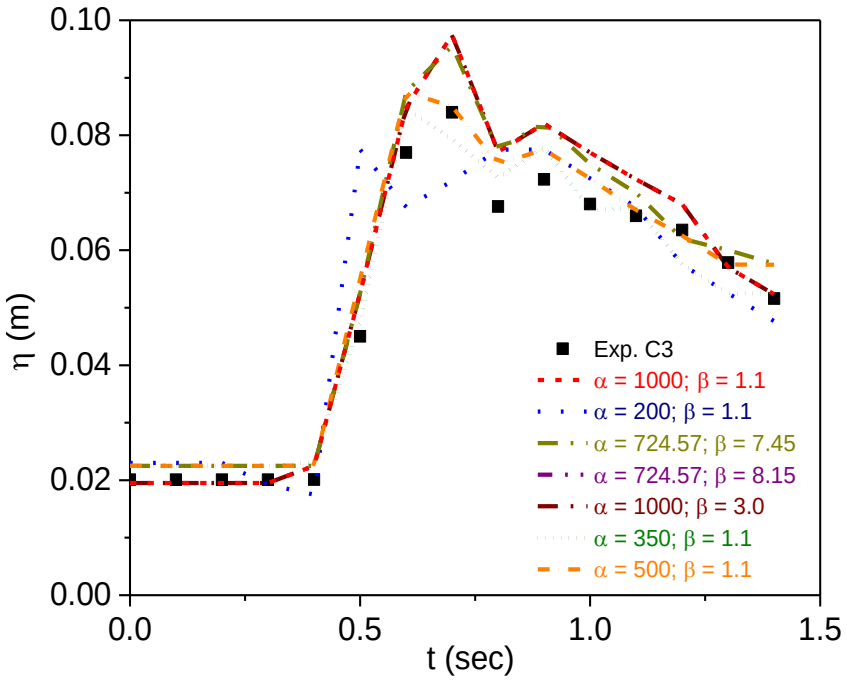

Figure 24. Comparison of measured and simulated wave heights for Case 3 (short porous obstacles) using Forchheimer model at location x = 1.18 m and y = 0.08 m.

Table 9. Simulation results of short porous obstacle Case 3 with Forchheimer method.

		Liu et al. (1999)	**Van Gent (1995)**	**Lara et al. (2011)**	**Lara et al. (2011)**	**Wu and Hsiao (2013)**	**Pramukti (2017)**
smallest grid size (mm)		Δx = 4 Δy = 4 Δz = 5					
Total grid number		268×40×80 = 857,600					
α , β		**200 , 1.1**	**1000 , 1.1**	**724.57 , 7.45**	**724.57 , 8.15**	**1000 , 3.0**	**500 , 1.1**
Wave height	Measured $\bar{\eta}$, η_{max} (m)	0.0502, 0.0840					
	Predicted $\bar{\eta}$, η_{max} (m)	0.0517, 0.0775	0.0548, 0.0975	0.0555, 0.0955	0.0555, 0.0955	0.0548, 0.0975	0.0540, 0.0875
	Δ	**1.4%, 8.4%**	**6.9%, 13.9%**	**8.2%, 12.1%**	**8.2%, 12.1%**	**6.9%, 13.9%**	**5.6%, 4.0%**
$\overline{\Delta t}$ (sec)		0.0007	0.0005	0.0005	0.0005	0.0004	0.0004
Computational time		26.8 hr	18.7 hr	17.9 hr	17.8 hr	18.7 hr	19.6 hr

Figure 25 compares the measured and simulated wave heights by the Forchheimer model for Case 4 at location x = 1.18 m and y = 0.08 m. The permeability constant α = 500 and the inertia factor β = 1.1 was set for Case 4. The difference between the simulated and measured average wave heights η was Δ = 1.2%. The difference between the simulated and measured maximum wave heights η was Δ = 6.7% (see Table 10). The simulation shows good results and can represent the results of experiments.

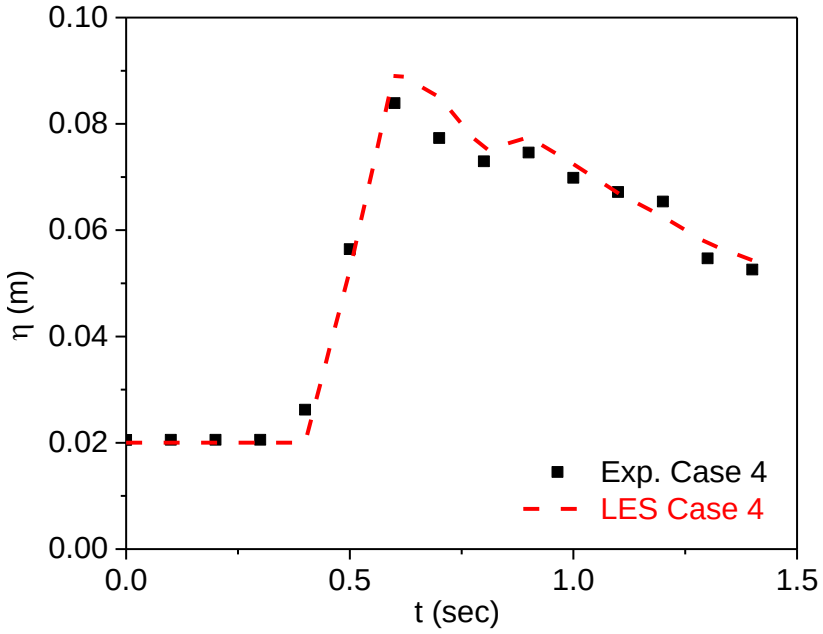

Figure 25. Comparison of measured and simulated wave heights for Case 4 (tall porous obstacles, h_f = 0.20 m, porosity n = 0.5) with the coefficients α = 500 and β = 1.1.

Table 10. Simulation results of short porous obstacle Case 4 with Forchheimer method.

		Grid A
smallest grid size (mm)		Δx = 4 Δy = 4 Δz = 5
Total grid number		857,600 268×40×80
α , β		500 , 1.1
Wave height	Measured $\bar{\eta}$, η_{max} (m)	0.0522, 0.0839
	Predicted $\bar{\eta}$, η_{max} (m)	0.0529, 0.0899
	Δ	**1.2%,** **6.7%**
$\overline{\Delta t}$ (sec)		0.0005
Computational time		24.1 hr

Figure 26 and Table 11 compares the simulated wave heights for all cases at location x = 1.18 m and y = 0.08 m. The wave height of Case 2 is higher than others. It is because the wave hit the solid obstacle and jump up. In addition, the phenomena cause the uncertainity in the measured wave height.

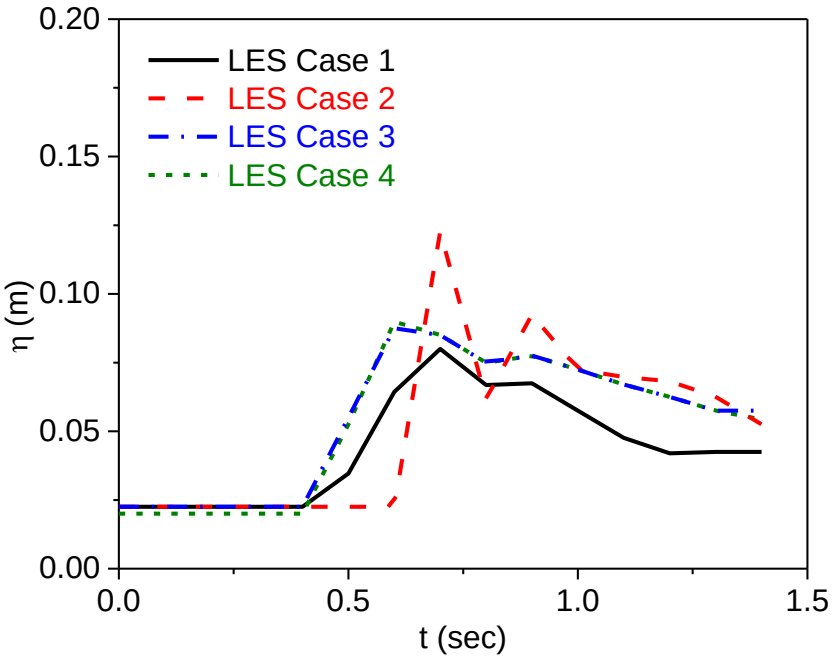

Figure 26. Comparison of simulated wave heights at location x = 1.18 m and y = 0.08 m for all cases.

Table 11. Simulation results of maximum and average wave height for all cases.

		Case 1	**Case 2**	**Case 3**	**Case 4**
Total grid number		268×40×80 = 857,600			
Wave height	Measured η_{max} , $\bar{\eta}$ (m)	0.0751, 0.0417	0.0954, 0.0457	0.0840, 0.0502	0.0838, 0.0522
	Predicted η_{max} , $\bar{\eta}$ (m)	0.0800, 0.0439	0.1378 , 0.0501	0.0875, 0.0540	0.0899, 0.0528
	Δ	**6.2%, 4.9%**	**4.7%, 4.0%**	**4.0%, 5.6%**	**6.7%, 1.2%**
$\overline{\Delta t}$ (sec)		0.0005	0.0006	0.0004	0.0004
Computational time		10.4 hr	13.5 hr	19.6 hr	24.1 hr

Table 12 compares the average error at location x = 1.18 m for all cases. The average error of the maximum wave height is defined as:

$$E(\%) = \frac{1}{n}\sum_{i=1}^{n}\frac{\left|\eta_{p,i} - \eta_{m,i}\right|}{\eta_{m,i}} \tag{17}$$

where $\eta_{p,i}$ and $\eta_{m,i}$ are the predicted and measured wave height at time t = 0.1 x i sec, and the total data number n = 14. The average error for Case 1, 2, 3 and 4 were 12.7%, 10.0%, 7.8% and 7.1%, respectively.

Table 12. Prediction errors for all four cases at location x = 1.18 m.

t	**Case 1**		**Case 2**		**Case 3**		**Case 4**	
(sec)	η_P	η_m	η_P	η_m	η_P	η_m	η_P	η_m
0.1	0.0225	0.0205	0.021	0.0201	0.0225	0.0201	0.0200	0.0206
0.2	0.0225	0.0205	0.021	0.0201	0.02253	0.0201	0.0200	0.0206
0.3	0.0225	0.0205	0.021	0.0201	0.0225	0.0201	0.0225	0.0206
0.4	0.0225	0.0205	0.021	0.0201	0.02314	0.0201	0.0165	0.0262
0.5	0.0346	0.0375	0.021	0.0201	0.0475	0.0450	0.0525	0.0564
0.6	0.0644	0.0712	0.021	0.0201	0.0847	0.0770	0.0899	0.0839
0.7	0.0800	0.0751	0.1378	0.1314	0.0794	0.0840	0.0850	0.0773
0.8	0.0668	0.0602	0.0409	0.0669	0.0726	0.0676	0.0750	0.0730
0.9	0.0675	0.0618	0.0951	0.0831	0.0780	0.0723	0.0775	0.0746
1	0.0575	0.0475	0.0778	0.0776	0.0670	0.0680	0.0725	0.0699
1.1	0.0476	0.0396	0.0720	0.0634	0.0674	0.0660	0.0670	0.0672
1.2	0.0420	0.0392	0.0710	0.0598	0.0576	0.0635	0.0625	0.0654
1.3	0.0425	0.0368	0.0599	0.0529	0.0525	0.0579	0.0575	0.0547
1.4	0.0425	0.0323	0.0503	0.0458	0.0525	0.0516	0.05435	0.0526
E (%)	**12.7**		**10.0**		**7.8**		**7.1**	

Figure 27, 28, and 29 illustrates the simulated velocity vectors on the central plane (y = 0.08 m) of the flume at six different times from t = 0.5 ~ 1.0 sec. The spatial distributions of the free surface elevation corresponding velocity fields. When the wave hit the obstacles, strong turbulent flows occur and lift up the water level.

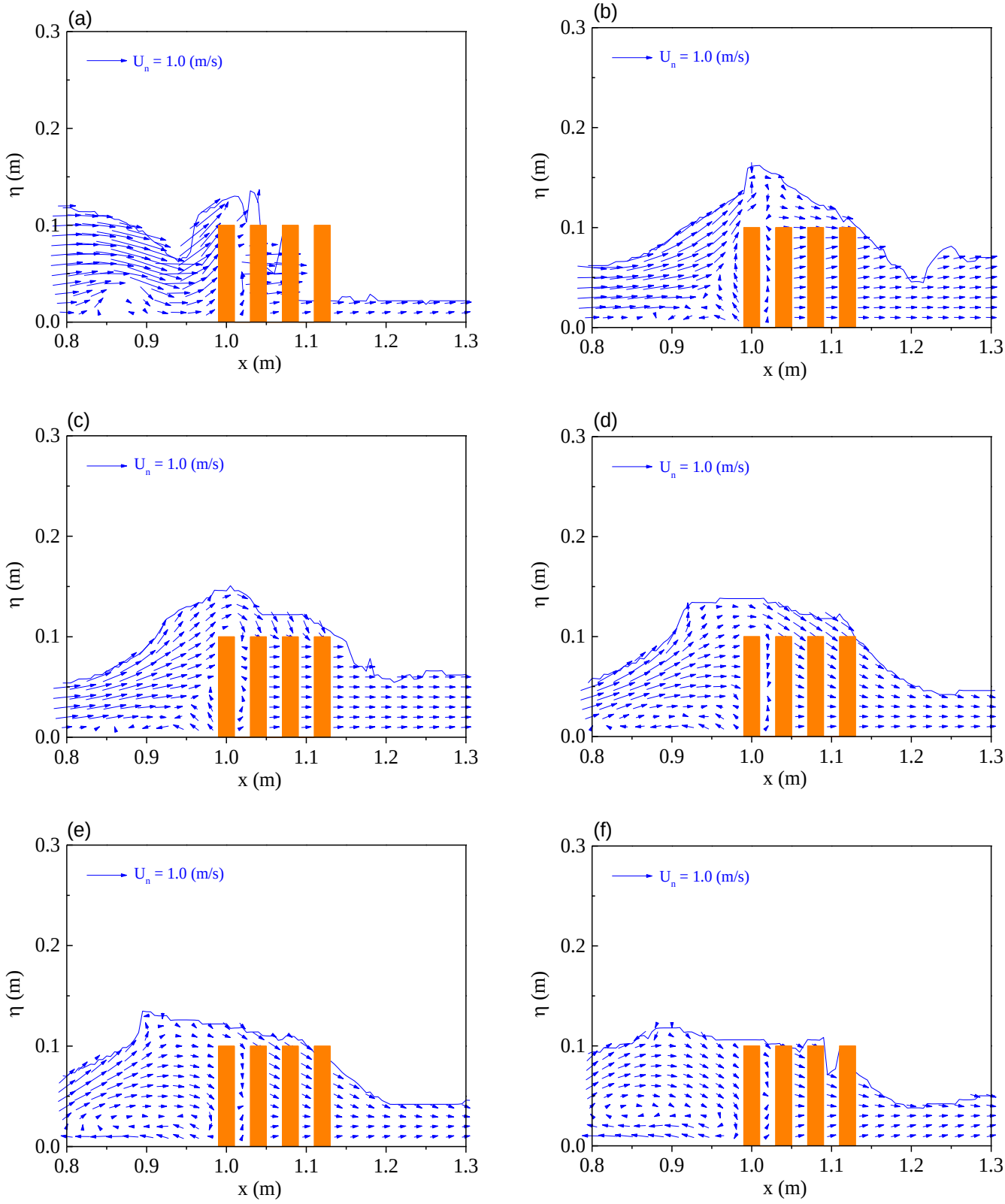

Figure 27. Velocity vectors on the central plane (y = 0.08 m) of the flume for Case 3 (short porous obstacles) uses solid method, h_o = 0.26 m; h_1 = 0.02 m; h_f = 0.10 m. (a) t = 0.5 s; (b) t = 0.6 s; (c) t = 0.7 s; (d) t = 0.8 s; (e) t = 0.9 s; (f) t = 1.0 s.

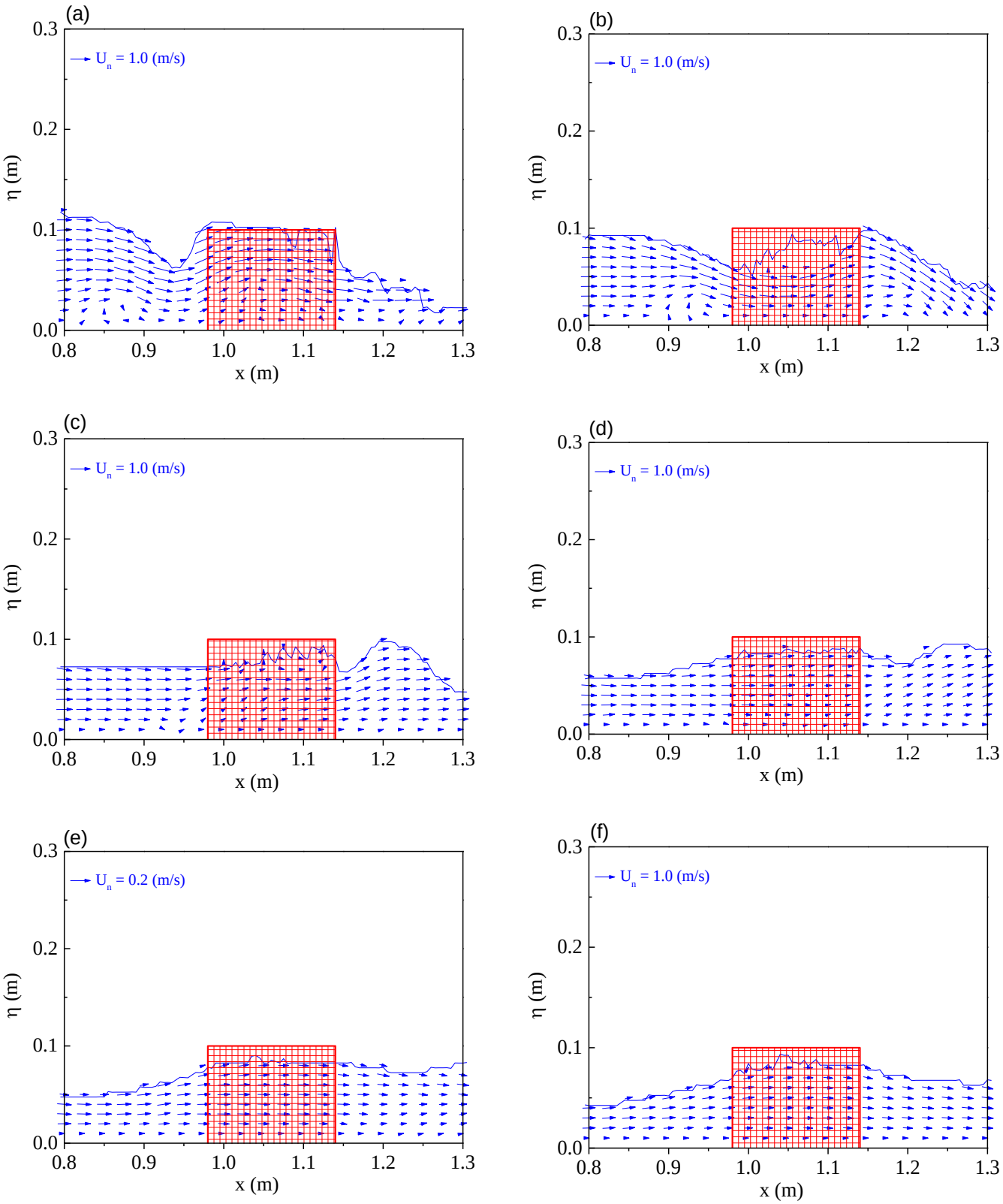

Figure 18. Velocity vectors on the central plane (y = 0.08 m) of the flume for Case 4 (tall porous obstacles, h_f = 0.10 m). (a) t = 0.5 s; (b) t = 0.6 s; (c) t = 0.7 s; (d) t = 0.8 s; (e) t = 0.9 s; (f) t = 1.0 s.

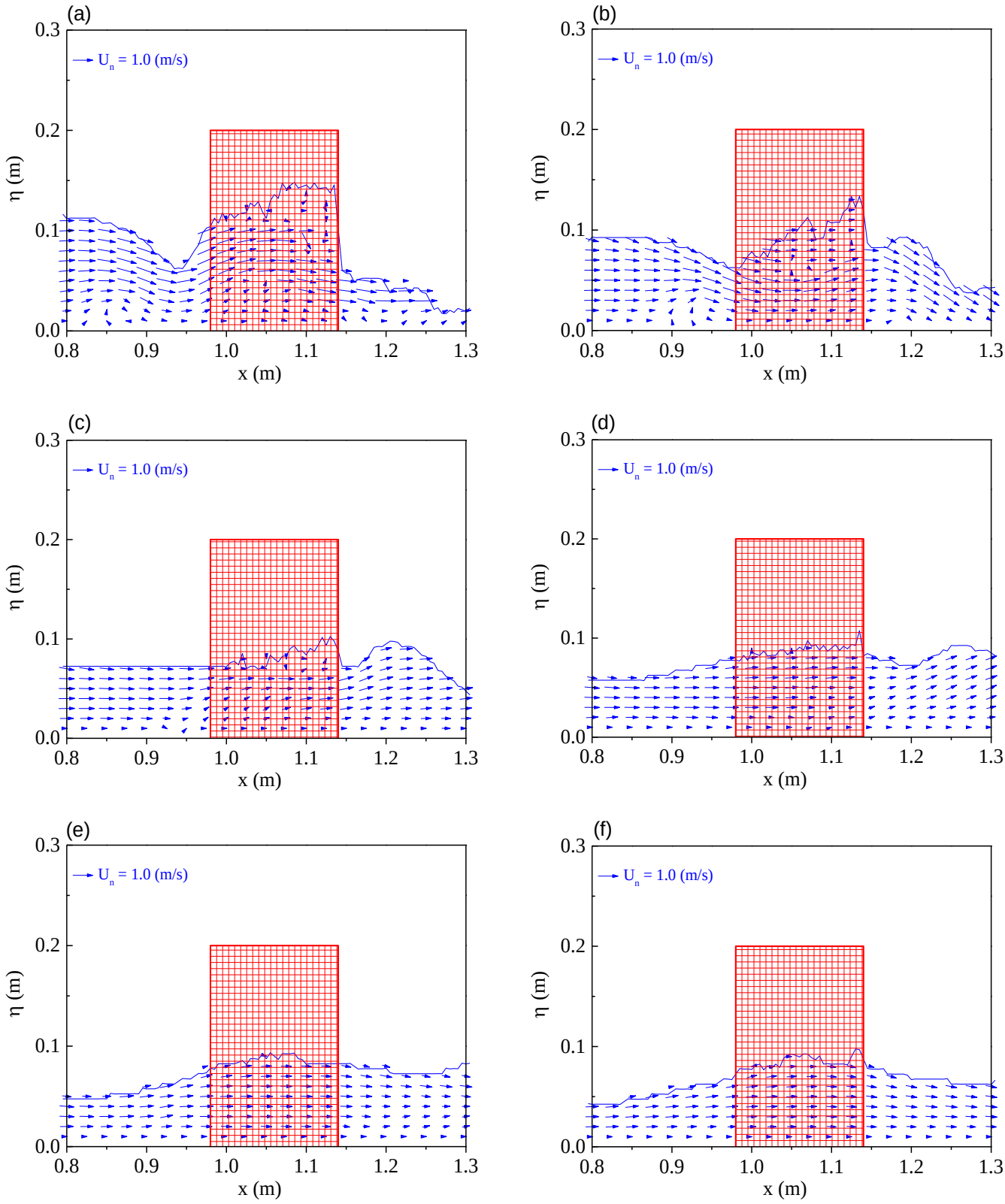

Figure 229. Velocity vectors on the central plane of the flume for Case 4 (tall porous obstacles). (a) t = 0.5 s; (b) t = 0.6 s; (c) t = 0.7 s; (d) t = 0.8 s; (e) t = 0.9 s; (f) t = 1.0 s.

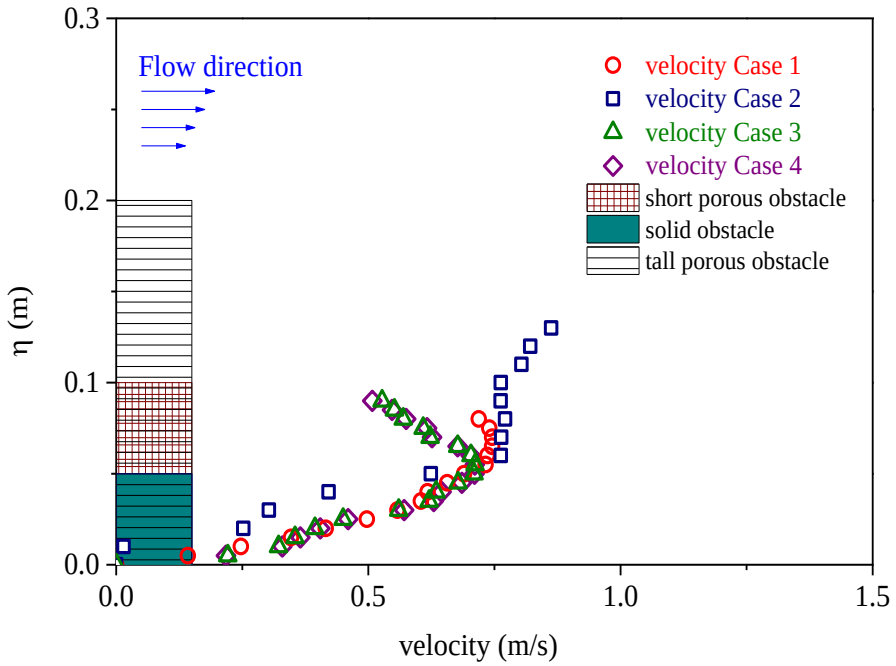

Figure 30. Comparison of instantaneous velocity behind the obstacles on the central plane of the flume at location x = 1.18 m at the same time t = 0.7 sec.

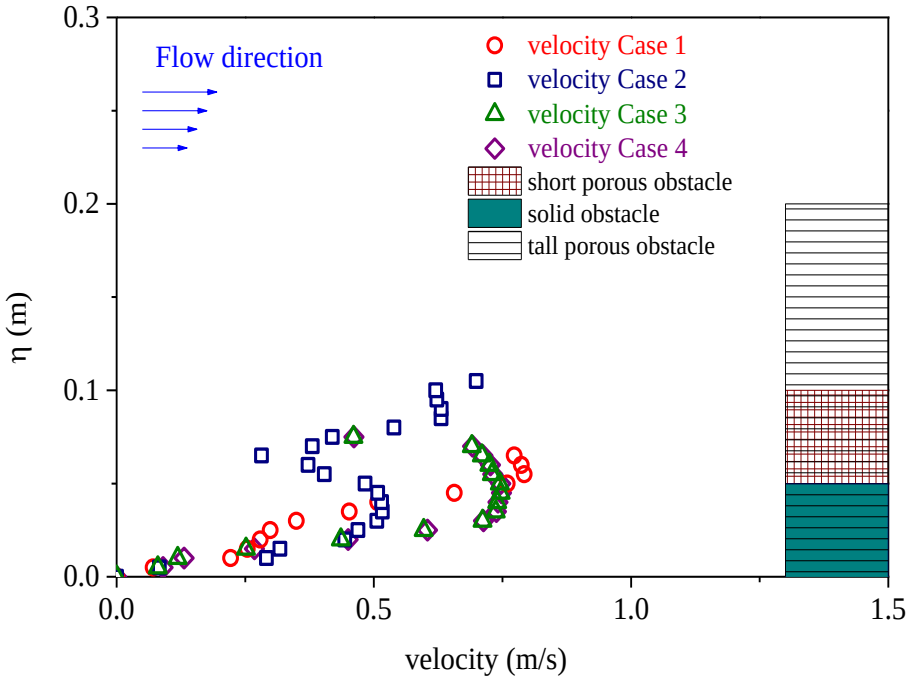

Figure 31. Comparison of instantaneous velocity in front of the obstacles on the central plane of the flume at location x = 0.92 m at the same time t = 0.7 sec.

Figure 30 and 31 compares the simulated instantaneous velocities at location x = 1.18 m for all cases at the same time. For Figure 30, shows the velocity distribution behind the obstacles. Case 1 obviously has the largest velocity, the maximum velocity is U = 0.75 m/s. The maximum velocity Case 2 is U = 1.01 m/s. The velocity distributions of Cases 3 and 4 are similar, and the maximum velocities were around U = 0.70 m/s. In other words, the porous obstacle can reduce the velocity effectively and Figure 31 shows the velocities distributions in front of the obstacle for all four cases. The velocity profiles were very similar and yet there is a change.

4.4. Drag Coefficient (C_D)

The validated Large Eddy Simulation model was used to investigate the interaction of free surface flow and porous obstacle. A series of numerical simulation were carried out to evaluate the effect of solid and porous obstacles on the dambreak flow. The simulated results of average and maximum wave heights are discussed.

Momentum integration method can be used to calculate the force acting on the object in a flow field. It is based on the momentum equation, and it has been used in wake flow, boundary layer flow and jet flow. In steady flow, the momentum equation can be simplified as:

$$F_x = \rho_{water}\left[\int_{up} U^2\,dA - \int_{down} U^2\,dA\right] \tag{18}$$

where F_x is the drag experienced by the water flow, U is velocity and $A = bh_f$ is the frontal area of the obstacle.

$$F_x = \rho_{water} b\left[\int_0^{h_f} u_{up}^2(z)\,dz - \int_0^{h_f} u_{down}^2(z)\,dz\right] \tag{19}$$

where ρ_{water} = 1000 kg/m^3 is the density of water, u_{up} and u_{down} are the velocity upstream and downstream of the obstacles, respectively.

The simulation results show that the flow through porous media is very well approximated by Forchheimer model (1901). The drag force is caused by the fluid impinging upon the obstacles. The drag force is a function of the fluid density and velocity, and the dimensionless drag coefficient is defined as:

$$C_D = \frac{F_x}{0.5\rho_{water}U_o^2 A} = \frac{F_x}{0.5\rho_{water}U_o^2 (b \cdot h_f)} \quad (20)$$

where $U_o = (gh_o)^{0.5} = 1.60$ m/s is a characteristic velocity of the dambreak flow.

Figure 32 shows the drag coefficients of dambreak flow through obstacles for Case 2, Case 3 and Case 4. Case 3 and Case 4, the value of drag coefficient is relatively similar. The highest values occurred at t = 0.80 sec, $C_d = 0.28$ for Case 3 and $C_d = 0.14$ for Case 4. There are some negative values in the Case 2, it is due to upstream point is too close to the obstacle. So, the velocity in the upstream tend to be smaller than in the downstream, due to the backflow.

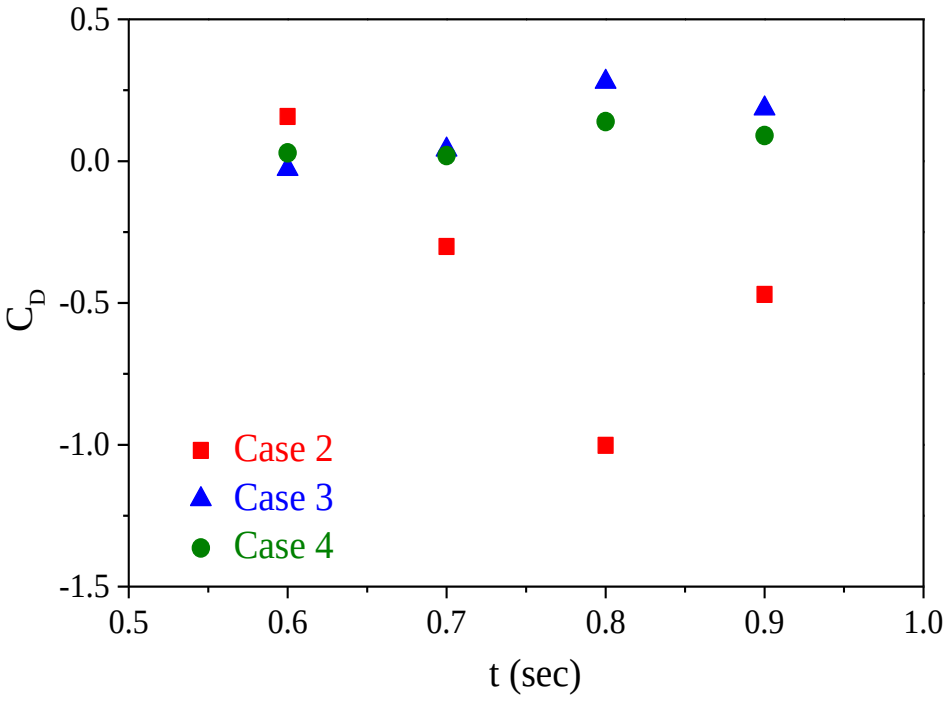

Figure 32. Drag coefficients of dambreak flow through obstacles at different times.

This page is intentionally left blank